Journal of Physical Science, Vol. 28(3), 19–40, 2017

Tailoring the Chemical and Structural Properties of Graphene Oxide Nanoplatelets Synthesised at Room Temperature with Different Processing Times

Guat Yee Toh,[1] Hui Lin Ong,[1*] Hong Ngee Lim,[2] Nay Ming Huang,[3] Hazizan Md Akil,[4] Al Rey Villagracia,[5] Gil Nonato C. Santos[5] and Hooi Ling Lee[6]

[1]School of Materials Engineering, Universiti Malaysia Perlis,
Kompleks Pusat Pengajian Jejawi 2, 02600 Arau, Perlis, Malaysia
[2]Chemistry Department, Faculty of Science, Universiti Putra Malaysia,
43400 UPM Serdang, Selangor, Malaysia
[3] Low Dimensional Materials Research Centre, Physics Department,
University of Malaya, 50603 Kuala Lumpur, Malaysia
[4]School of Materials and Mineral Resources Engineering, Engineering Campus,
Universiti Sains Malaysia, 14300 Nibong Tebal, Pulau Pinang, Malaysia
[5]Department of Physics, De La Salle University,
2401 Taft Avenue, Manila 0922, Philippines
[6]School of Chemical Sciences, Universiti Sains Malaysia,
11800 USM Pulau Pinang, Malaysia

[*]Corresponding author: hlong@unimap.edu.my

Published online: 15 November 2017

To cite this article: Toh, G. Y. et al. (2017). Tailoring the chemical and structural properties of graphene oxide nanoplatelets synthesised at room temperature with different processing times. *J. Phys. Sci.*, 28(3), 19–40, https://doi.org/10.21315/jps2017.28.3.2

To link to this article: https://doi.org/10.21315/jps2017.28.3.2

ABSTRACT: *A simplified Hummer's method was successfully used in synthesising graphene oxide nanoplatelets. These nanoplatelets were synthesised at room temperature at various processing times (24 h, 72 h, and 120 h). Ultraviolet visible spectroscopy (UV-vis) showed that all synthesised graphene oxide nanoplatelets suspensions have similar broad shoulder absorbance at a wavelength of 300 nm. Furthermore, similar functional groups were detected by Fourier transform infrared spectroscopy (FTIR) across all types of graphene oxide nanoplatelets structures. The effect of processing time on the thickness of the sheet size was interpreted through topology using atomic force microscopy (AFM). The structural properties of graphene oxide nanoplatelets were evaluated using X-ray diffraction (XRD). The results showed a slight increase in the interlayer spacing with no sharp distinction in the crystallinity for graphene oxide nanoplatelets at longer processing times. The ratio of carbon to oxygen composition on the surface of each synthesised graphene oxide nanoplatelet was computed using the X-ray photoelectron spectroscopy*

(XPS). Field emission scanning electron microscopy (FESEM) was used to determine the morphology of the nanoplatelets. Three steps of degradation occurred during the thermogravimetric analysis (TGA). Degradation peaks were identified using differential scanning calorimetry (DSC). Electrical properties were characterised using the four-probe conductivity method. It can be concluded that properties such as sheet size, thickness, morphology and electrical conductivity of the graphene oxide nanoplatelets can be tuned by varying the processing time while maintaining its chemical characteristics.

Keywords: Graphite, graphene oxide, oxidation, electrical properties, thermal stability

1. INTRODUCTION

Graphene, made of a single layer of carbon atoms which tends to exist in sheet or ribbons, is a two-dimensional (2D) material having length and width but mere one-atom-thick nanosheets that are arranged in a honeycomb or hexagonal lattice.[1–3] It is a unique material due to the sp^2 hybridisation of carbon atoms, lending a promising characteristic in condensed matter and high-energy physics.[4] However, there is still no simple way to obtain graphene in a single-step process from pristine graphite. One of the methods being used is to synthesise it from graphene oxide (GO) through a reduction process. Unlike graphene, GO is a monolayer of graphite oxide that can be synthesised through three different methods: Brodie method, Staudenmaier method, and Hummer's method.[5–7] The Brodie method uses graphitic powder with potassium chlorate ($KClO_3$) in concentrated nitric acid (HNO_3).[8] The Staudenmaier method replaced the Brodie method using a single-step approach to produce well-oxidised graphite with longer oxidation time. Moreover, a higher amount of excess oxidising agent and additive of concentrated sulfuric acid (H_2SO_4) is utilised during the continuous process without the need to use nitric acid.[9] These two methods require longer processing times, and are risky compared to the Hummer's method, which uses a shorter time during the oxidation process. In this method, potassium permanganate ($KMnO_4$) and sodium nitrate ($NaNO_3$) are used as oxidising agents in concentrated sulfuric acid (H_2SO_4).[10]

Regardless of the method used in producing GO, the structure of the GO nanoplatelets is still unknown. Yet, different structures of GO have been proposed, such as Hofmann structure, Ruess structure, Scholz-Boehm structure, Nakajima-Matsuo structure, Lerf-Klinowski structure, and Décány structure.[11] Generally, the proposed structure of GO contains epoxies and hydroxyl groups within the graphene sheets, and carbonyl and carboxyl groups at the edge of the sheets.[12] Theoretically, the structure and properties of GO depend highly on the synthesis method and the degree of oxidation. However, there are no studies found catering to the effects of processing time on its structure and properties.

This study investigates the effects of processing time during the production of GO on its properties using the simplified Hummer's method at room temperature. Unique properties of GO such as morphology, carbon to oxygen ratio (C/O ratio) and electrical conductivity were determined and examined within the requirement of GO in carbon-based theory. Such a consideration would be relevant in polymer nanocomposites when GO nanoplatelets are used as fillers.

2. EXPERIMENTAL

2.1 Materials

Graphite crystalline flakes (Code: 3061) were supplied by Asbury Graphite Mill, Inc (Asbury, New Jersey, US). Sulfuric acid (H_2SO_4) 95%–97% for analysis EMSURE® ISO concentration, phosphoric acid (H_3PO_4) 85%, potassium permanganate ($KMnO_4$) or permanganic acid potassium salt, hydrogen peroxide (H_2O_2) and hydrochloric acid (HCl) with analytical grade were supplied by Merk KGaA, Darmstadt, Germany. These were used as received. Deionised water was used throughout the experiment.

2.2 Synthesis of GO

GO was synthesised according to the simplified Hummer's method at room temperature.[13] During the process, 360 ml of H_2SO_4 and 40 ml of H_3PO_4 (ratio 9:1) were stirred at room temperature until it became homogeneous. Next, 3 g of graphite flakes were added into the chemical mixture, followed by 18 g of $KMnO_4$. The solvent mixture was stirred at room temperature for different processing times: 24 h (GO-24), 72 h (GO-72), and 120 h (GO-120). The mixture was poured into a beaker filled with ice cubes containing 27 ml of H_2O_2. The final product was centrifuged and washed with 1 M of HCl three times, and then washed repeatedly using deionised water until the pH was around 4–5.

2.3 Characterisation Techniques

The ultraviolet visible spectrum (UV-vis) of each GO was measured using Hitachi's U-2800 model, a UV-vis spectrophotometer with absorption scanning region from 200 nm to 400 nm. The concentration of each solution was fixed for the purpose of comparative analysis.

Fourier transform infrared spectroscopy (FTIR) analysis was carried out precisely using Perkin Elmer's spectrometer. GO was dried in an oven at 60°C for 24 h before characterisation. Potassium bromide (KBr) powder was mixed with the dried

GO, and grounded until it turned into fine particles. The mixture was pelletised using a hydraulic press at an 8-ton pressure for 3 min. Potassium bromide pellets containing 1 wt% GO mixture were prepared for FTIR. The spectrum for each specimen was scanned 32 times from 450 cm^{-1} to 4000 cm^{-1} spectral region with 4 cm^{-1} resolutions.

The topology of each GO was studied using atomic force microscopy (AFM) with SPA 400, SII Nano Technology, Japan equipped with SI-DF2 cantilever tip under non-contact mode at room temperature. It was spin-coated at 1500 rpm for one minute on a silicon wafer substrate. The crystalline structure and X-ray diffraction pattern of each GO was recorded using Bruker D2 PHASER, at a scanning rate of 0.033°s^{-1} in a 2θ range from 5° to 40° with Cu Kα radiation (λ=1.5148 Ă). The 1-mm diverging slit and 8-mm receiving slit were used. The GO nanoplatelets were spin-coated at 800 rpm for 1 min on quartz glasses. Meanwhile, the interlayer spacing of the GO was retrieved using Bragg's law:

$$n\lambda = 2d.\sin\theta \quad (1)$$

The elements in GO, such as carbon (C), hydrogen (H), and oxygen (O), were characterised using the X-ray photoelectron spectroscope (XPS) technique with Kratos Axis DLD.

The morphologies of GO nanoplatelets were characterised using field emission scanning electron microscopy (FESEM) model S-36 (Leica Cambridge Ltd. with Leo Supra 35 VP system). The GO was spin-coated at 1500 rpm for 1 min on a silicon wafer, and scanned at a magnification of 3000X.

Thermogravimetric analysis (TGA), Mettler Toledo, gas controller GC 200, STAR^e system was used to determine the thermal stability of GO (~10 mg) at a temperature range of 30°C to 800°C with heating rate 10°C/min at 1 atm. A thermal analysis on GO (~5 mg) using the differential scanning calorimetry (TA DSC Q-10) technique was performed in nitrogen atmosphere from 30°C to 250°C with a heating rate 10°C/min.

The electrical conductivity of each GO was determined using the Keithley 2400 semiconductor characterisation system (four-probe method), as presented in Figure 1. The liquid- based GO was casted on a 2.5 cm × 2.5 cm plastic mould and dried in an oven for 24 h at 50°C. The thin films have a thickness of around 35 µm. A constant bias current of 0.1 A was applied to measure the voltage over the GO thin film. Electrical conductivity (σ) was calculated using 1/R, where R is resistivity. Using Equation 2, the resistivity of the specimens was calculated based

on the average gradient slope obtained from the current (I) versus voltage (V) from five specimens.

$$R = [\text{Resistance } (\Omega) \times \text{area } (A)] / \text{thickness of the thin film } (t) \quad (2)$$

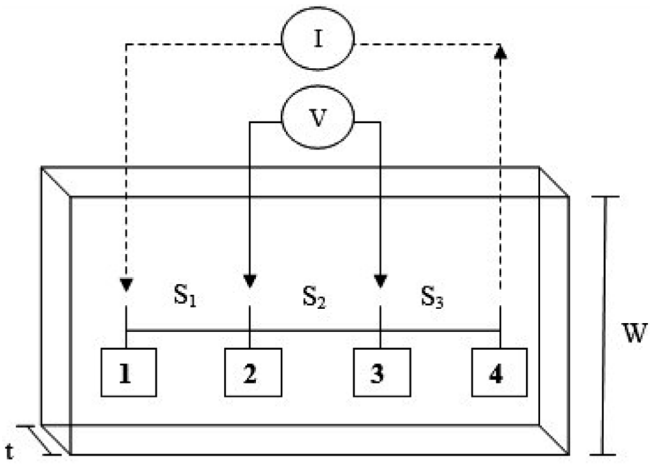

Figure 1: Schematic diagram of four points probe test setup.[14] Probe 1 and Probe 4 carry current (I), Probe 2 and Probe 3 measure voltage (V).

3. RESULTS AND DISCUSSION

3.1 Mechanism of GO Formation

The synthesising of GO involved several chemicals (as shown in Figure 2), which started by using graphite flakes as the raw materials. Oxidising agent such as potassium permanganate ($KMnO_4$) will react with strong acid, sulfuric acid (H_2SO_4) during the oxidation of graphite materials. According to Hummer's method used in this study, the combination between the chemical reaction of oxidising agent and acid were illustrated as below:[11]

$$KMnO^4 + 3\ H_2SO_4 \rightarrow K^+ + MnO_3^+ + H_3O^+ + 3\ HSO$$

$$MnO_3^+ + MnO_4^- \rightarrow Mn_2O^7 \text{ (dimanganese heptoxide)}$$

This formation of dark red oil or dimanganese heptoxide was known as an explosive material when the temperature of the reaction is greater than 55°C or placed together with organic compounds.[11] However, with the present of oxidising

agent ($KMnO_4$) and strong acid (H_2SO_4) in graphite flakes, the appearance of diol functional groups onto the surface of graphite flakes was identified. Due to the strong acid used, it is believed that formation of holes in the graphene basal plane will appear. Thus, protecting agent such as phosphoric acid (H_3PO_4) was added into the synthesis process, so that the elimination of hole formation on the surface of graphite will be minimised. As shown in Figure 2, phosphoric acid was reacting with the diol functional groups through in-situ reaction to prevent hole formation. Chelation occurred between the protecting agent and diol functional groups, thus increasing the formation of GO from the graphite flakes.[15,16]

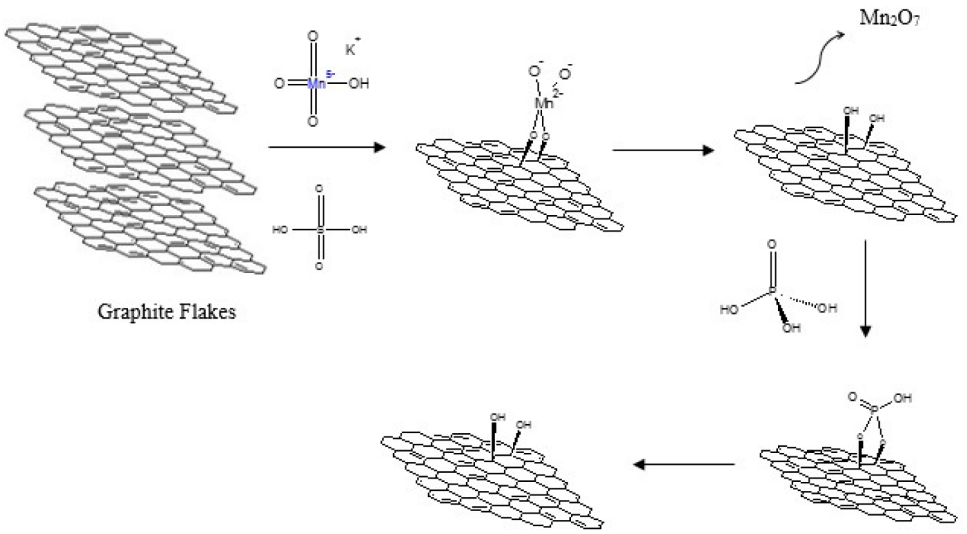

Figure 2: Mechanism of synthesising GO.

3.2 Ultraviolet Visible Spectroscopy (UV-vis)

The GO nanoplatelets were examined by using UV-vis spectroscopy at a fixed volume. Based on the absorbance spectra (0.1 cm path length), two absorption features could be observed in the spectra of all types of GO; a main peak was found at 230 nm for each specimen due to the changes in electronic transition involving π electrons, transition of C=C,[17] together with a characteristic shoulder at around 300 nm, which attributed to n electrons in the π* excited state for -C=O-, carbonyl groups.[18] As shown in Figure 3, the absorption peak for GO-24, GO-72, and GO-120 were found at 0.859, 1.166 and 1.095, respectively. GO nanoplatelets with a 72-h processing time have the highest absorption at same concentration. This indicates that more functional groups were found on the basal plane of GO.

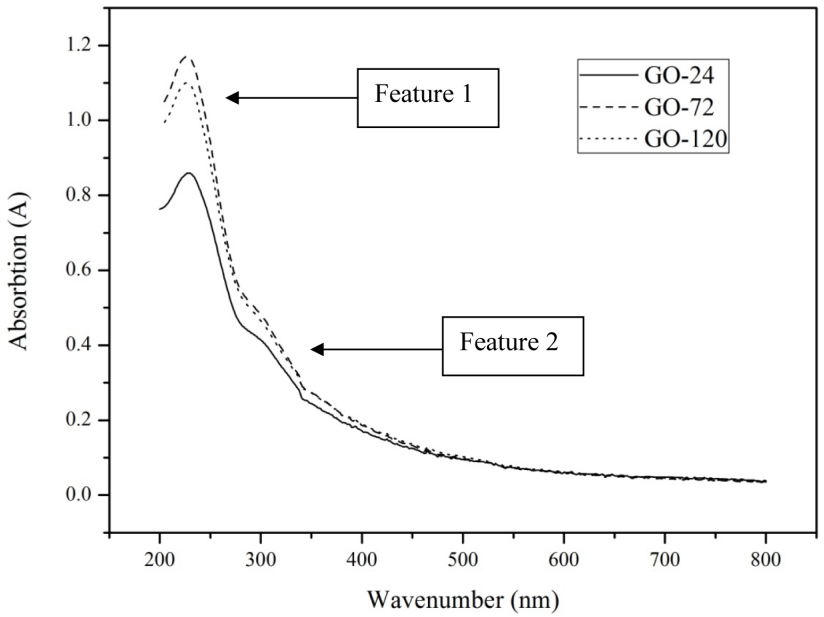

Figure 3: UV-vis absorption spectra (10 mm path length) of 24 h, 72 h and 120 h processing time of GO nanoplatelets.

3.3 Fourier Transform Infrared Spectroscopy

The Fourier transform infrared spectroscopy (FTIR) spectral analysis was performed quantitatively to confirm the chemical structure of all the functional groups. Figure 4 summarises the FTIR spectra of the graphite flakes for all types of synthesised GO. A series of procedures was introduced to quantitatively analyse the FTIR spectra:[20]

1. Baseline correction of the selected region;
2. The selected spectra were multiplied by –1; set y is set to 0 to get positive value for the bands;
3. Deconvolution of the band; and
4. Measurements and spectra processing (chemimetrics) on the area under the curve with non-aromatic band : total band, where subtraction is used to remove the area of aromatic band.

As shown in Figure 4, the graphite spectra contained three dominant characteristic bands at wavenumber 3451–3149 cm^{-1}, 1656 cm^{-1}, and 1111 cm^{-1} that correspond to the O-H stretch, C=C stretch, and C-O-C band. For GO with a 24-h

processing time, the main features can be confirmed by the bands at 3211 cm^{-1} (O-H hydroxyl group), 1728 cm^{-1} (C=O carboxyl groups), and 1625 cm^{-1} (C=C aromatic groups), as well as the bands at 1151 cm^{-1} and 1028 cm^{-1}, which corresponds with the C-O in the epoxide group. Same spectrum peaks appeared in case of 72 h and 120 h of processing time of GO. Thus, it can be concluded that the synthesised GO specimens exhibit all the important characteristic peaks.[21]

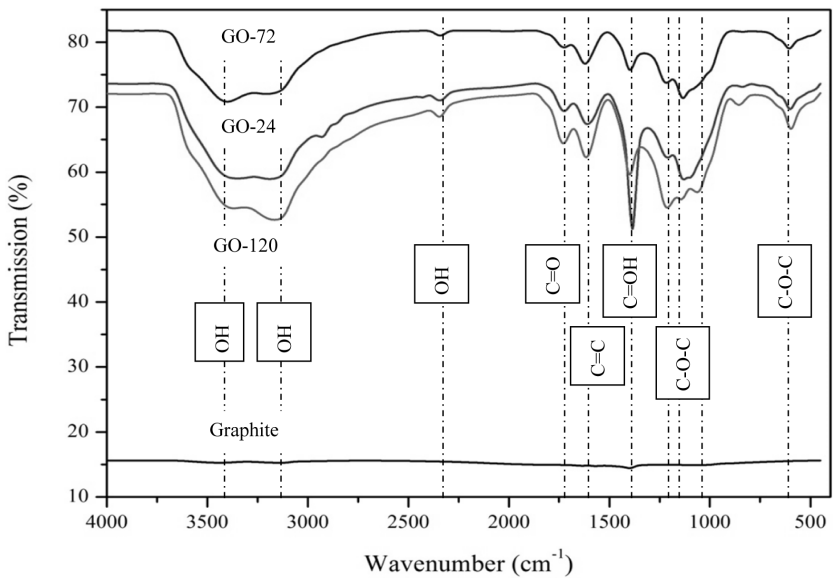

Figure 4: FTIR spectra of GO with different oxidation time.

In contrast, a very broad peak (3000–3600 cm^{-1}) was generated from the stretching vibrations of hydroxyl group (-OH) from carboxylic acid (COOH) and water (H_2O). As the processing time was increased, the oxygen-related band ratio to total area was determined. For the aromatic region with wavenumber 1475–1690 cm^{-1}, the ratios are 5.139, 5.673, and 6.356 for the 24-h, 72-h and 120-h processing times, respectively. This indicates that processing time affects the area ratio.

3.4 Atomic Force Microscopy

The topography of the GO specimens is clearly illustrated in Figure 5. A typical sheet-like morphology of GO can be easily distinguished based on the colour contrast of the sheets. The monolayer of GO has a brighter colour in contrast when compared to aggregation or self-assembly of two or three layers of GO. Moreover, wrinkles were found on the surface of GO due to the stacking or agglomeration of graphene sheets.

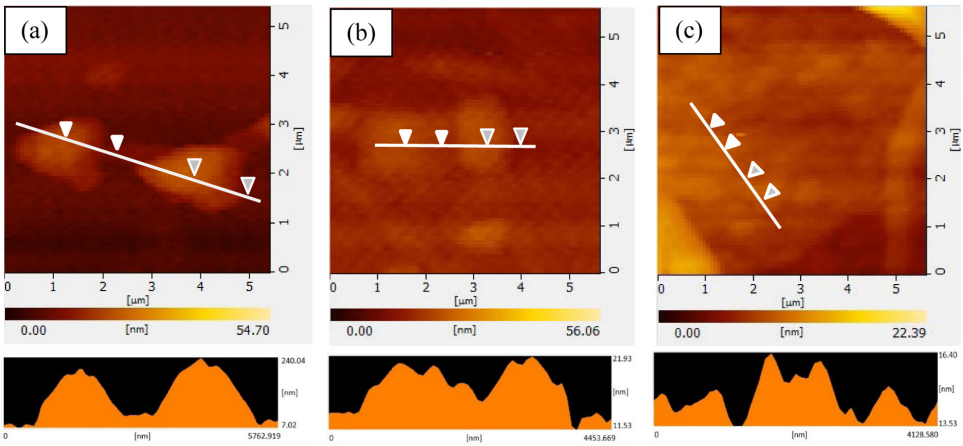

Figure 5: Topology of 3D view for GO nanoplatelets after coated on the silicon wafer according to different processing times: (a) GO-24, (b) GO-72 and (c) GO-120.

Based on the AFM height profile analysis, the mean thickness of the exfoliated GO sheets were noted as 0.89 nm, 1.32 nm, and 1.79 nm for GO-24, GO-72 and GO-120, respectively. This result was derived from a statistical evaluation, which is in agreement with the published AFM data on the minimum thickness of GO fragments on the surface of mica, suggested to be 1.3 nm.[19–21]

The van der Waals thickness of the single-layer graphene sheet is about 0.34 nm, corresponding to the interlayer spacing of the graphite.[21] However, as discussed earlier, the oxidation level of GO has a great effect on the thickness of the graphene sheets. This is because of the presence of covalently bonded oxygen and the displacement of the sp^3 hybridised carbon atom slightly above and below the original graphene basal plane.[22]

3.5 Structural Analysis

X-ray diffraction (XRD) patterns were used to provide a conclusive proof for determining the change in the structure in terms of layer distances, crystallinity and crystallography of GO from graphite when the processing time is varied. Results are summarised in Table 1. All diffractograms are taken in reflection mode, and the corresponding interlayer distance is calculated using Bragg's law ($\lambda = 1.54$ Ă), from 5° and 40° for 2θ. It can be seen in Figure 6 that the XRD pattern of the graphite flakes shows a diffraction peak at $2\theta = 26.91°$ (002) planes with an interlayer spacing of about 0.33 nm corresponding to the layer-to-layer distance.[23] This indicates the abundance of unoxidised graphite flakes.[24] Furthermore, when the processing time is increased, the intensity of the peak at $2\theta = 26.91°$ starts

decreasing and finally disappears for 120 h of processing time. When the oxidation time is prolonged, distinct diffraction peaks are formed at 2θ = 9.45°, 8.53°, and 8.58° (represented in Figure 7) for GO with an interlayer spacing, d = 0.94 nm, 1.04 nm, and 1.03 nm, respectively. The interlayer distance of the graphite flakes and the various oxidation levels of GO nanoplatelets were increased throughout the chemical oxidation process.[25] During the oxidation process, oxygen functional groups, phosphate (PO_4^-) and sulphate (SO_4^-), insert themselves into the graphene layers. However, a slight reduction in interlayer spacing was observed from the 72 h processing time to 120 h processing time due to the behaviour of the phenol related band.[26]

Table 1: Summary of structural analysis on GO based on different processing times.

	Pristine graphite	GO-24	GO-72	GO-120
d-spacing (nm)	0.33	0.94	1.04	1.03
Crytallite size (Å)	6.9	6.3	6.7	6.7
Crystallinity (%)	28.5	24.1	36.6	40.8
Amorphous (%)	71.5	75.9	63.4	59.2

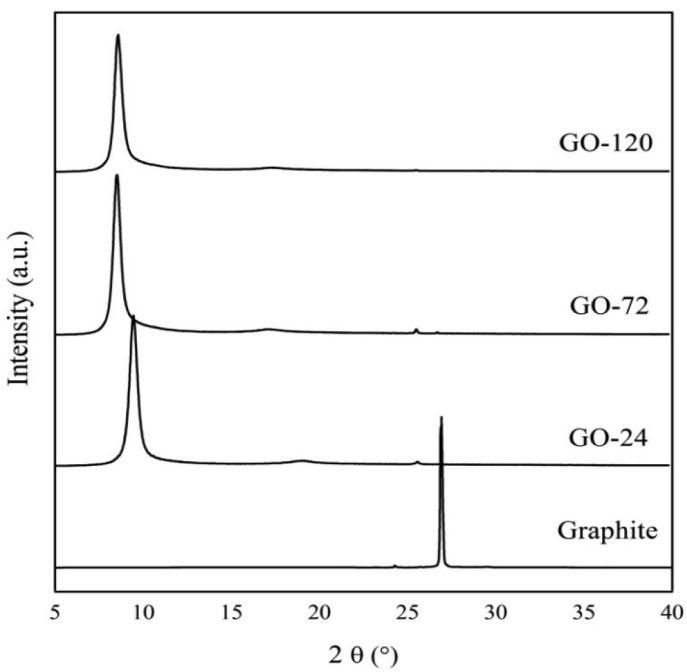

Figure 6: XRD pattern of graphite and various oxidation level of GO (GO-24, GO-72 and GO-120).

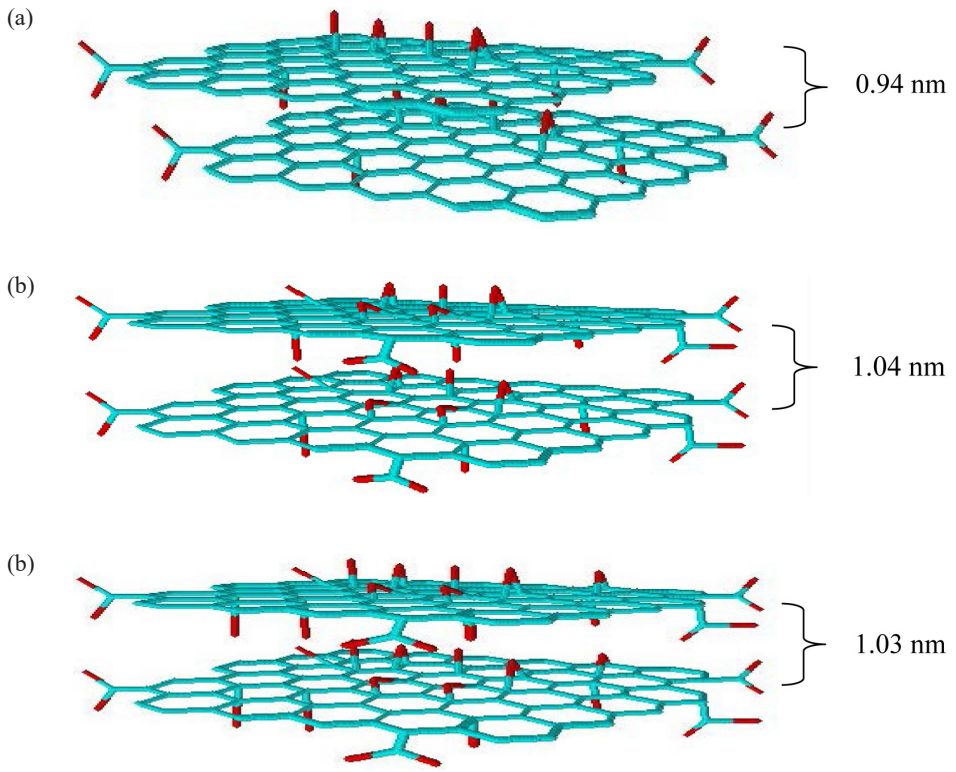

Figure 7: Schematic diagram of layered structure GO at different processing times with (a) GO-24, (b) GO-72 and (c) GO-120.

Based on the results, it can be said that the interlayer spacing for 72 h and 120 h of GO is significantly larger than the one for 24 h processing time. This indicates that a longer oxidation time leads to larger interlayer spacing of graphite oxide by intercalating oxide functional groups on the carbon basal plane. The increment on the interlayer spacing between different oxidation levels of GO is due to the introduction of different levels of oxygen on to the carbon basal plane via a chemical oxidation reaction.[13,27] The crystallite sizes of GO at different processing times are 6.3 Å, 6.7 Å, 6.7 Å for GO-24, GO-72 and GO-120, respectively. These values were determined using the Scherrer Equation 3:

$$\tau = \frac{K\lambda}{\beta \cos \theta} \tag{3}$$

where τ is represented by crystallite size; K is the dimensional shape factor (K=1); λ is the X-ray wavelength; β is the line broadening at half the maximum intensity after the subtraction of instrument line broadening; and θ is the Bragg angle.

It can be concluded that the crystallite sizes of GO are approximately equal to each other (~6.7Å) at higher processing times. The percent crystallinity of each synthesised GO was determined by DIFFRAC.EVA. The results are listed in Table 1 using Equation 4.

$$\text{Percent crystallinity} = \frac{\text{Total area of crystalline peak}}{\text{Total area of all peak}} \times 100 \quad (4)$$

3.6 X-ray Photoelectron Spectroscopy (XPS)

XPS was employed to quantitatively determine the chemistry of the material at the surface.[28,29] Figure 8 presents the XPS survey spectra of GO nanoplatelets. Based on the results, only oxygen, carbon, and a slightly traced amount of sodium were detected in all three prepared specimens. The amounts of elements and functional groups computed by XPS are shown in Table 2. The carbon to oxygen (C/O) atom ratio was about 2.86, 2.49, and 2.28 for 24 h, 72 h and 120 h of processing time, respectively. This indicates that the oxidation level of specimens decreases slightly.

Table 2: Functional groups of GO nanoplatelets computed by XPS.

Specimens	C (at %)	O (at %)	C/O ratio	C=C (at %)	C-O / C-O-C (at %)	C=O (at%)	O-C=O (at %)
24 h	74.08	25.92	2.86	57.06	34.71	3.72	4.50
72 h	71.33	28.67	2.49	44.49	43.33	4.69	4.40
120 h	69.54	30.46	2.28	46.03	45.10	5.21	3.65

The structure of GO consists of the following: epoxide and hydroxyl groups, on the basal plane, are the major components; and carbonyl and carboxyl groups at the edge of the GO structure are the minor components.[30] Table 2 shows the elemental composition of the synthesised specimens. This further proves that most of the functional groups containing oxygen, such as epoxide and hydroxyl, appear at the carbon skeleton during the oxidation process with higher atomic percentage. However, very few oxygen atoms existed at the edge of the GO. Two main peaks in GO specimens were identified in Figure 8(b) to (d). The major peak at 284.8–284.6 eV is assigned to carbon atom (C=C) with sp^2 hybridised orbitals. The other peak at 286.4–286.6 eV is assigned to epoxide (C-O-C) and hydroxyl (C-O) with sp^3 hybridised orbitals.[31,32] Minor peaks of ketone or quinone, C=O, (287.2–288.0 eV) and carboxylate, O-C=O (288.2–289.3 eV), were determined according to the peak-fitting method using the Casa XPS software.[29] The longer the processing time, the more C=C bonding in GO is decomposed. This leads to the formation of C-C bond, and change of the spectra from sp^2 to sp^3 hybridised.[32]

Based on the XPS analyses, the element concentration of carbon and oxygen, at different processing times in the GO series could be calculated quantitatively using Equation 5:[31]

$$n = \frac{I_{\text{element (C or O)}} / S_{\text{element (C or O)}}}{I_{\text{total element}} / S_{\text{total element}}} \times 100 \quad (5)$$

where $I_{\text{element (C or O)}}$ is the integrated intensities of either carbon or oxygen peak in C1s XPS spectra; $S_{\text{element (C or O)}}$ is the sensitivity factor of either carbon or oxygen peak in C1s XPS spectra; and $I_{\text{total element}}$ and $S_{\text{total element}}$ are the intensity and sensitivity factor of the total element (carbon and oxygen) in C1s XPS, respectively.

The element concentration calculated is listed in Table 3. It confirms that prolonging the processing time decreases the amount of carbon element; and increases the amount of oxygen element.

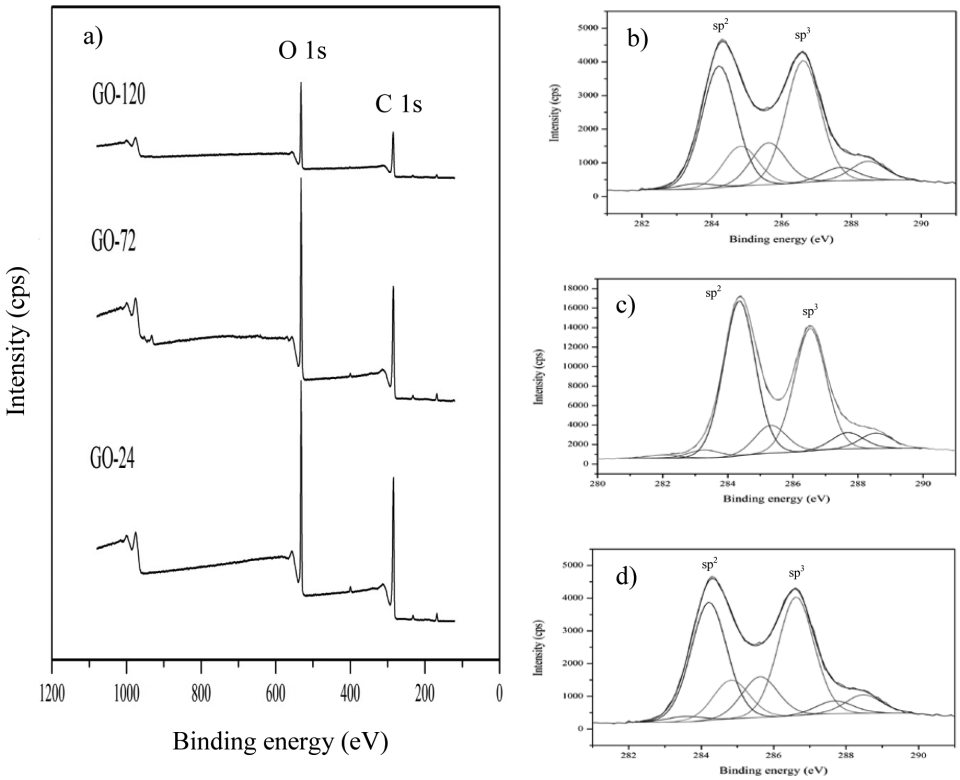

Figure 8: C 1s XPS spectra of (a) all types of GO nanoplatelets; and enlargement of banding energy from 280–290 eV for (b) 120 h; (c) 72 h; (c) 24 h.

Table 3: Carbon and oxygen element from different processing time of GO nanoplatelets.

	24 h	72 h	120 h
Carbon element, C	0.638	0.637	0.591
Oxygen element, O	0.218	0.363	0.408

Note: Sensitivity factor, S for carbon is 1 and oxygen is 2.93.[29]

3.7 Morphologies of GO Nanoplatelets

Based on the micrographs shown in Figure 9, it was found that the lateral dimension of GO decreases in case of a longer oxidation time.[33] However, due to the short oxidation time for GO, some graphite particles can still be found in the micrographs. Based on the presented specimens, the optimum oxidation time that can be concluded is 72 h. GO-72 has an average dimension of an exfoliated GO sheet. Based on the FESEM images for GO-120, it could be seen that the lateral dimension of the proposed GO is quite small. This is due to the plausible mechanism of overly oxidised on the GO sheets, which leads to the tearing of the sheets.[13]

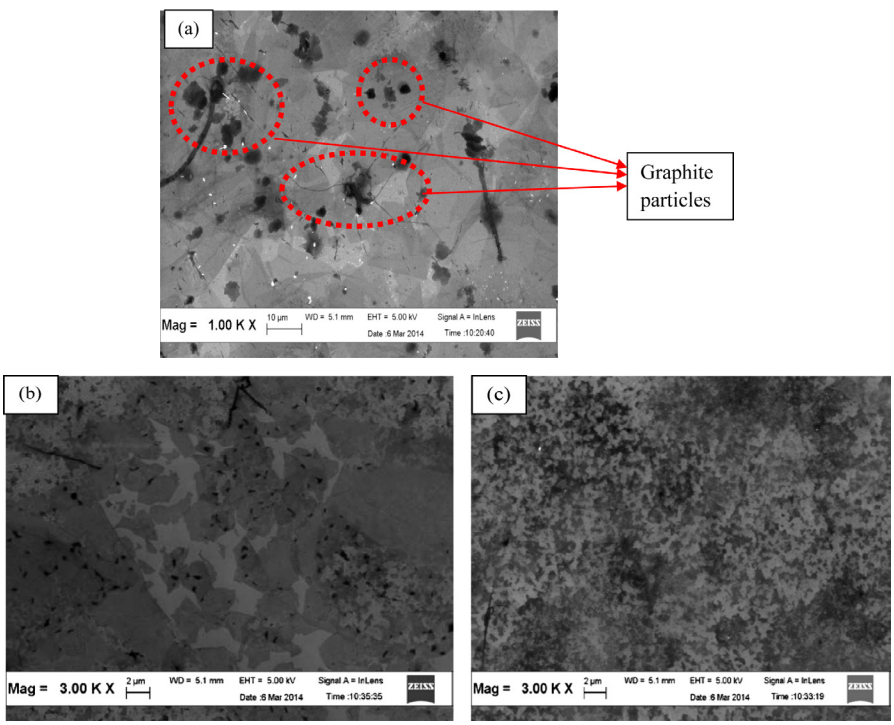

Figure 9: FESEM micrographs for (a) GO-24, (b) GO-72 and (c) GO-120 of synthesised GO at magnification 3000X.

3.8 Thermal Analysis

The thermogravimetric analysis (TGA) results provide further information about the different processing times of GO. Figures 10 and 11 show the TGA and derivative thermogravimetric (DTG) results for GO-24, GO-72, and GO-120. The results indicate that there are three steps of degradation of GO that occur during the process at four main temperatures near 200°C, 300°C, 500°C, and 700°C along with a water related peak near 100°C at first dominant temperature. On heating, the GO started losing mass, this is associated with the elimination of loosely bound or adsorbed water and gas molecules.

The first two dominant temperatures near 200°C and 300°C correspond to the decomposition of functional groups. The second two dominant temperatures near 600°C and 700°C correspond to the decomposition of carbon backbones. The peak has a burning temperature around 200°C. This can be ascribed to hydroxyl groups.[34] The peak with a higher burning temperature around 300°C has a stronger bond, which can be attributed to carboxyl groups. This is because of the existing double bond between carbon and oxygen of the carboxyl group. This is a stronger bond than the single bond between carbon and oxygen atoms of the hydroxyl group. Studies have shown that in the temperature range from 30°C to 700°C, sp^2 carbon backbones appear due to the decreased integrated area at higher oxidation times, and completely disappear after a long oxidation time.[34]

It can be concluded that the oxidation time of GO will affect the thermal stability of the material due to the functional groups attached at the carbon basal graphene sheets. Based on the results shown in Figure 10, the remaining residues are about 25.78% for GO-24, 18.68% for GO-72 and 16.04% for GO-120, respectively. These indicated that the remaining residue that appeared is potassium element generated from potassium manganate, which did not react completely to from GO.[35,36] Thus, it can be concluded that the influence of potassium residues that act as catalyst in the oxidation reaction will be reduced proportionally with the increase in the synthesising time.

The DSC curves of GO at a heating rate of 10°C/min are shown in Figure 12. The differential scanning calorimetry (DSC) of GO shows different correlated degradation peaks centred at 173°C, 166°C, and 170°C for GO-24, GO-72, and GO-120, respectively. The peaks are caused by the decomposition of the organic groups on the GO sheets and evolution of water (H_2O), carbon monoxide (CO), and carbon dioxide (CO_2).[37]

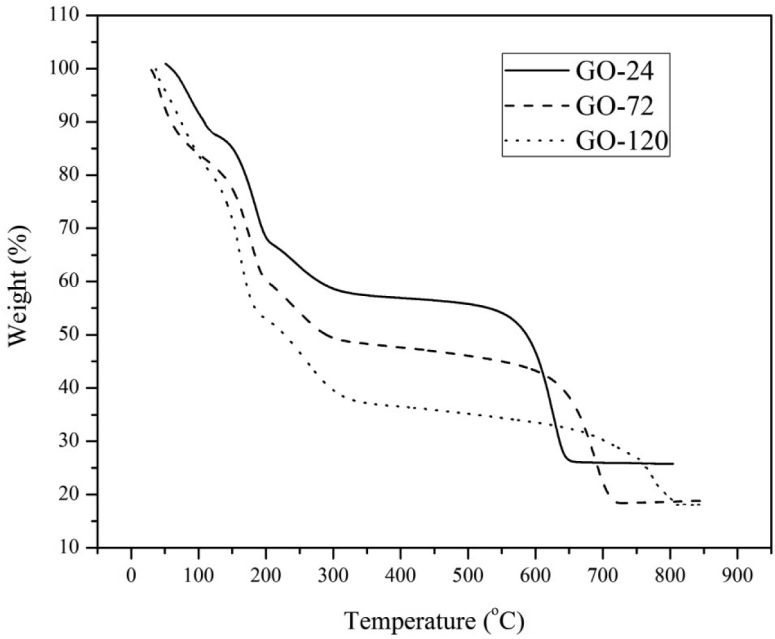

Figure 10: Thermogravimetric diagram based on different processing times of synthesised GO.

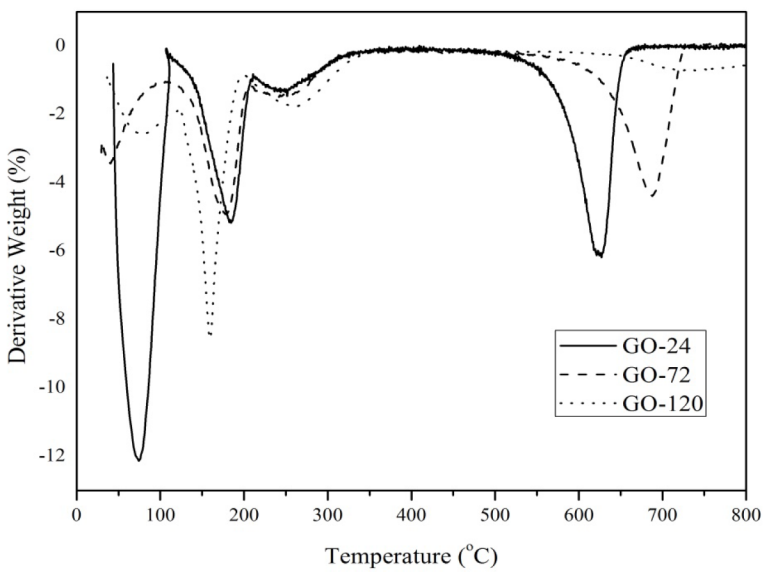

Figure 11: Derivative thermogravimetric diagram based on different processing times of synthesised GO.

Based on the results, the 24 h processing time of GO-24 has the highest degradation peak at 173.3°C. This is due to the presence of functional group with less oxygen on the carbon basal plane. This phenomenon principally means that more oxidation and longer exfoliation introduce more defects and functional groups on the GO sheets. This reduces the size of the GO sheets with more functional groups. Furthermore, it lowers the decomposition temperature.[38] However, as per results shown in Figure 12, GO-120 has a higher decomposition temperature compared to GO-72. The peak at 170°C is attributed mainly to the decomposition of the oxygenic groups to CO_2, and the sharp peak at 166°C of GO-120 is mainly due to the catalytic dehydration of the epoxy, hydroxyl, and C-H species.[39]

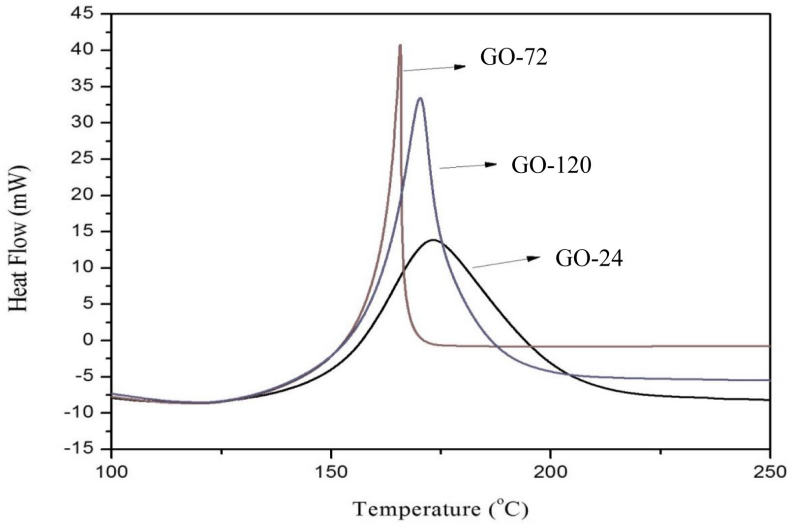

Figure 12: DSC thermogram based on different processing times of GO.

3.9 Electrical Conductivity

In terms of electrical conductivity, GO is often described as an electrical insulator due to the presence of the sp^3 hybridised bonding network in the structure. However, the conductivity of GO depends on many factors, such as the degree of oxidation, surface chemistry of the GO,O/C ratio,impurities in the GO, and exfoliation of the graphite layers.[27,40] As shown in Figure 13, the resistance value obtained from the slope of current (I) versus voltage (V) is 1.09×10^{-2} kΩ for GO-24, 1.49×10^{-2} kΩ for GO-72 and 1.64×10^{-2} kΩ for GO-120. These results are in line with the argument that the oxygen atoms found in the GO functional groups highly affect the resistance of the material. This has also been proved in the previous XPS results. When the processing time is increased, the oxygen content on the surface of the GO increases simultaneously together with the resistance.

Theoretically, the electrical conductivity is the reciprocal of electrical resistivity. Figure 14 shows that the electrical conductivity of GO-24 gives the highest conductivity among all types of synthesised GO. This is due to the lowest oxygen functional groups in the structure. From the experimental data, it can be seen that the conductivity of the GO gradually changes with the effect of C:O ratio that is found in the structure.[27]

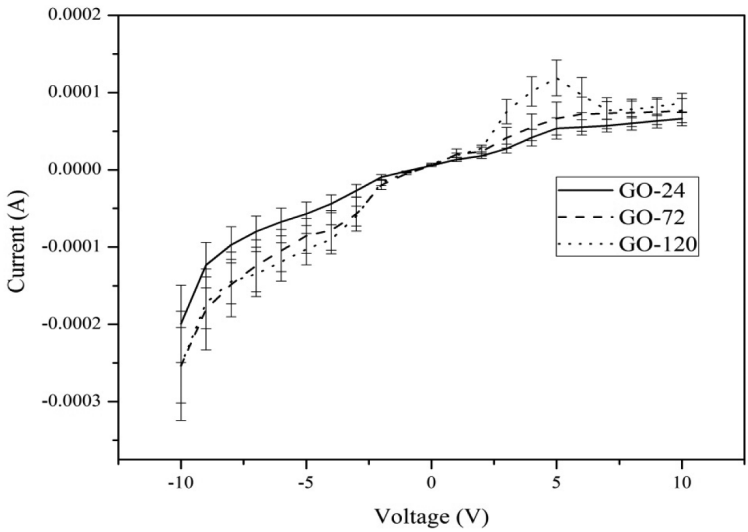

Figure 13: Plot of current (I) versus voltage (V) for different processing times of GO at constant bias current of 0.1 A.

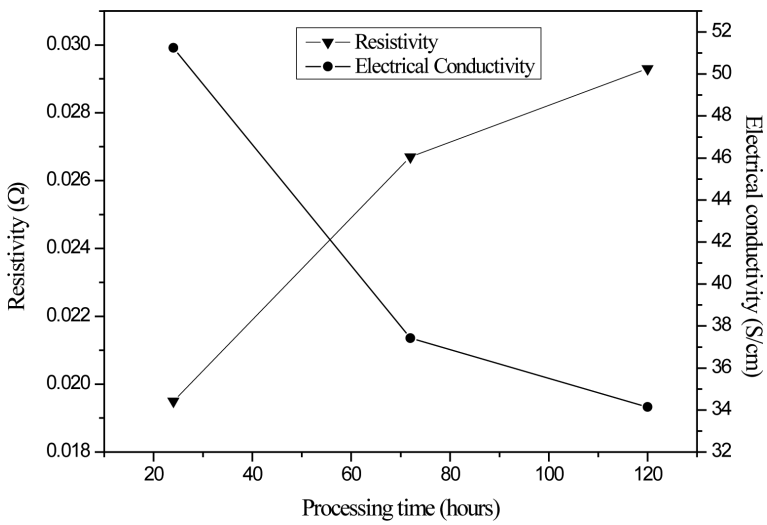

Figure 14: Electrical conductivity of GO at various processing times.

4. CONCLUSION

GO nanoplatelets were successfully prepared at room temperature using the simplified Hummer's method at different processing times. The characteristic shoulder peak at around 300 nm was found on all types of GO using UV-vis. Different absorption peaks were identified due to the effect of the size of GO sheets. These results were further confirmed by obtaining the surface morphology of the GO using FESEM. The relative amount of oxygen functional groups was estimated in FTIR using quantitative measurement. This showed that the ratio of oxygen related band increases when the processing time increases. A topology study using AFM concluded that longer processing times created the largest mean thickness for the sheet sizes of GO. Through X-ray diffraction, the interlayer spacing, crystallinity, and crystallite size were estimated using Bragg's law, and the percent of crystallinity based on the crystalline and amorphous region was determined using Scherrer equation. The interlayer spacing and crystallite size obtained at higher processing times were closely similar. However, the crystalline behaviour of GO is directly proportional to the processing time.

The XPS and CasaXPS data revealed that GO specimens have functional groups such as hydroxyl (-OH), epoxy group (O-C-O), carboxylate (O-C=O), and ketone (C=O) on the surface. The XPS spectra showed that all specimens have two kinds of carbon atoms: carbon atom with sp^2-hybridied orbital and carbon atom with sp^3-hybridised orbital. As the processing time is increased, the sp^3-hybridised orbital of carbon atoms also increased. The carbon element decreases when the processing time is longer. The thermal gravimetric analysis showed that the processing time of the GO affected the thermal stability of the material due to the functional groups at the edge of the carbon basal graphene sheets. More oxygen functional groups in the GO structure reduce the conductivity of the material. Overall, the surface chemistry of GO influences the sheet size, thickness, morphology, carbon to oxygen ratio, thermal stability properties, and electrical conductivity properties. However, each type of GO nanoplatelets produced at different processing times could be aimed as reinforcement in different applications. For example, the highest conductivity behaviour of GO-24 will be used as reinforcement in electronic application; larger sheets size of GO-72 could provide positive gas barrier behaviour in food packaging applications; and better thermal stability of GO-120 will be aimed as new opportunities in electronics devices.

5. ACKNOWLEDGEMENTS

The authors would like to express their gratitude to the Government of Malaysia for the financial support extended via the Project Grant - Fundamental Research

Grant Scheme (FRGS) with project number: 9003-00374 and the Ministry of Higher Education Malaysia for the MyBrain15-MyPhD Scholarship.

6. REFERENCES

1. Sankeshwar, N. S., Kubakaddi, S. S. & Mulimani, B. G. (2013). Thermoelectric power in graphene. In M. Aliofkhazraei (Ed.). *Thermoelectric power in graphene, advances in graphene science*. Rijeka, Croatia: InTech, 217–271, https://doi.org/10.5772/56720.
2. Katsnelson, M. I. (2012). *Graphene: Carbon in two dimensions*. Cambridge: Cambridge University Press, https://doi.org/10.1017/CBO9781139031080.
3. Weiss, N. O. et al. (2012). Graphene: An emerging electronic material. *Adv. Mater.*, 24(43), 5782–5825, https://doi.org/10.1002/adma.201201482.
4. Akhavan, O. & Ghaderi, E. (2012). Escherichia coli bacteria reduce graphene oxide to bactericidal graphene in a self-limiting manner. *Carbon*, 50(5), 1853–1860, https://doi.org/10.1016/j.carbon.2011.12.035.
5. Zhao, J., Liu, L. & Li, F. (2015). *Graphene oxide: Physics and applications.* London: Springer, https://doi.org/10.1007/978-3-662-47253-8.
6. Yanwu, Z. et al. (2010). Graphene and graphene oxide: Synthesis, properties and applications. *Adv. Mater.*, 22(46), 3906–3924, https://doi.org/10.1002/adma.201001068.
7. Ciszewski, M. & Mianowski, A. (2013). Survey of graphite oxidation methods using oxidizing mixtures in inorganics acids. *Chemik*, 67(4), 267–274.
8. Brodie, B. C. (1859). On the atomic weight of graphite. *Phil. Trans. Royal Soc. Lond.*, 149, 249–259, https://doi.org/10.1098/rstl.1859.0013.
9. Staudenmaier, L. (1898). Verfahren zur darstellung der graphitsäure. *Berichte der deutschen chemischen gesekkschaft*, 31(2), 1481–1487, https://doi.org/10.1002/cber.18980310237.
10. Hummers, W. S. & Offeman, R. E. (1958). Preparation of graphitic oxide. *J. Am. Chem. Soc.*, 80(6), 1339, https://doi.org/10.1021/ja01539a017.
11. Dreyer, D. R. et al. (2009). The chemistry of graphene oxide. *Chem. Soc. Rev.*, 39(1), 228–240, https://doi.org/10.1039/B917103G.
12. Sengupta, R. et al. (2011). A review on the mechanical and electrical properties of graphite and modified graphite reinforced polymer composites. *Prog. Polym. Sci.*, 36(5), 638–670, https://doi.org/10.1016/j.progpolymsci.2010.11.003.
13. Huang, N. M. et al. (2011). Simple room-temperature preparation of high-yield large-area graphene oxide. *Int. J. Nanomed.*, 6, 3443–3448, https://doi.org/10.2147/IJN.S26812.

14. Mironov, V. S. et al. (2007). Comparison of electrical conductivity data obtained by four-electrode and four-point probe methods for graphite-based polymer. *Polym. Test*., 26(4), 547–555, https://doi.org/10.1016/j.polymertesting.2007.02.003.
15. Eigler, S. & Hirsch, A. (2014). Chemistry with graphene and graphene oxide-challenges for synthetic chemists. *Angew. Chem. Int. Ed.*, 53(30), 7720–7738, https://doi.org/10.1002/anie.201402780.
16. Tour, J. M. & Kosynkin, D. V. (2012). Highly oxidized graphene oxide and methods for production thereof. U.S. Patent Application No. 13/321,623.
17. Gauglitz, G. & Tuan, V.-D. (2003). *Handbook of spectroscopy.* Weinheim: Wiley-VCH Verlag, https://doi.org/10.1002/3527602305.
18. Luo, Z. et al. (2009). High yield preparation of macroscopic graphene oxide membranes. *J. Am. Chem. Soc.*, 131(3), 898–899, https://doi.org/10.1021/ja807934n.
19. Kang, D. & Shin, H. S. (2012). Control of size and physical properties of graphene oxide by changing the oxidation temperature. *Carbon Lett.*, 13(1), 39–43, https://doi.org/10.5714/CL.2012.13.1.039.
20. Dideykin, A. et al. (2011). Monolayer graphene from graphite oxide. *Diam. Relat. Mater.*, 20(2), 105–108, https://doi.org/10.1016/j.diamond.2010.10.007.
21. Dong, X. et al. (2010). Ultra-large single-layer graphene obtained from solution chemical reduction and its electrical properties. *Phys. Chem. Chem. Phys.*, 12(9), 2164–2169, https://doi.org/10.1039/b914546j.
22. Singh, K., Ohlan, A. & Dhawan, S. K. (2012). *Polymer-graphene nanocomposites: Preparation, characterization, properties and applications.* In Ebrahimi, F. (Ed). *Nanocomposites - New trends and developments*. Rijeka, Croatia: InTech, https://doi.org/10.5772/50408.
23. Bykkam, S. et al. (2013). Synthesis and characterization of graphene oxide and its antimicrobial activity against Klebseilla and Staphylococus. *Int. J. Adv. Biotech. Res.*, 4(1), 142–146.
24. Tamás, S. et al. (2006). Evolution of surface functional groups in a series of progressively oxidized graphite oxides. *Chem. Mater.*, 18(11), 2740–2749, https://doi.org/10.1021/cm060258+.
25. Meng, L.-Y. & Park, S.-J. (2012). Preparation and characterization of reduced graphene nanosheets via pre-exfoliation of graphite flakes. *Bull. Korean Chem. Soc.*, 33(1), 209–214, https://doi.org/10.5012/bkcs.2012.33.1.209.
26. Guerrero-Contreras, J. & Caballero-Briones, F. (2015). Graphene oxide powders with different oxidation degree, prepared by synthesis variations of the Hummers method. *Mater. Chem. Phys.*, 153, 209–220, https://doi.org/10.1016/j.matchemphys.2015.01.005.

27. Krishnamoorthy, K. et al. (2013). The chemical and structural analysis of graphene oxide with different degrees of oxidation. *Carbon*, 53, 38–49, https://doi.org/10.1016/j.carbon.2012.10.013.
28. Fairley, N. (2009). *Casa XPS manual 2.3.15: Introduction to XPS and AES*. Devon: Casa Software.
29. Yan, H. et al. (2014). Effects of the oxidation degree of graphene oxide on the adsorption of methylene blue. *J. Hazard. Mater.*, 268, 191–198, https://doi.org/10.1016/j.jhazmat.2014.01.015.
30. Gao, X., Zhao, Y. & Chen, Z. (2013). *From graphene to graphene oxide and back - Graphene chemistry: Theoretical perspectives*. New York: John Wiley & Sons.
31. Shao, G. et al. (2012). Graphene oxide: The mechanisms of oxidation and exfoliation. *J. Mater. Sci.*, 47, 4400–4409, https://doi.org/10.1007/s10853-012-6294-5.
32. Lee, D. W. & Seo, J. W. (2011). Sp2/sp3 carbon ratio in graphite oxide with different preparation times. *J. Phys. Chem. C*, 115(6), 2705–2708, https://doi.org/10.1021/jp107906u.
33. Zhao, J. et al. (2010). Efficient preparation of large-area graphene oxide sheets for transparent conductive films. *Acs. Nano.*, 4(9), 5245–5252, https://doi.org/10.1021/nn1015506.
34. Jeong, H. K. et al. (2009). Tailoring the characteristics of graphite oxides by different oxidation times. *J. Phys. D: Appl. Phys.*, 42(6), 065418, https://doi.org/10.1088/0022-3727/42/6/065418.
35. Kim, F. et al. (2010). Self-propagating domino-like reactions in oxidized graphite. *Adv. Funct. Mater.*, 20(17), 2867–2873, https://doi.org/10.1002/adfm.201000736.
36. Krishnan, D. et al. (2012). Energetic graphene oxide: Challenges and opportunities. *Nano Today*, 7(2), 137–152, https://doi.org/10.1016/j.nantod.2012.02.003.
37. Qiu, S. L. et al. (2011). Effects of graphene oxides on the cure behaviors of a tetrafunctional epoxy resin. *Express Polym. Lett.*, 5(9), 809–818, https://doi.org/10.3144/expresspolymlett.2011.79.
38. Zhang, L. et al. (2009). Size-controlled synthesis of graphene oxide sheets on a large scale using chemical exfoliation. *Carbon*, 47(14), 3365–3380, https://doi.org/10.1016/j.carbon.2009.07.045.
39. Hong, Y., Wang, Z. & Jin, X. (2013). Sulfuric acid intercalated graphite oxide for graphene preparation. *Scient. Rep.*, 3, 3439, https://doi.org/10.1038/srep03439.
40. Lee, W. et al. (2013). Simultaneous enhancement of mchanicl, electrical and thermal properties of graphene oxide paper by embedding dopamine. *Carbon*, 65, 296–304, https://doi.org/10.1016/j.carbon.2013.08.029.